Printable Fabrication of Nanocoral-Structured Electrodes for High-Performance Flexible and Planar Supercapacitor with Artistic Design

*Yuanjing Lin, Yuan Gao, and Zhiyong Fan**

Planar supercapacitors with high flexibility, desirable operation safety, and high performance are considered as attractive candidates to serve as energy-storage devices for portable and wearable electronics. Here, a scalable and printable technique is adopted to construct novel and unique hierarchical nanocoral structures as the interdigitated electrodes on flexible substrates. The as-fabricated flexible all-solid-state planar supercapacitors with nanocoral structures achieve areal capacitance up to 52.9 mF cm^{-2}, which is 2.5 times that of devices without nanocoral structures, and this figure-of-merit is among the highest in the literature for the same category of devices. More interestingly, due to utilization of the inkjet-printing technique, excellent versatility on electrode-pattern artistic design is achieved. Particularly, working supercapacitors with artistically designed patterns are demonstrated. Meanwhile, the high scalability of such a printable method is also demonstrated by fabrication of large-sized artistic supercapacitors serving as energy-storage devices in a wearable self-powered system as a proof of concept.

The booming market of portable and wearable devices has aroused growing demand for energy-storage devices that combine both high performance and attractive form factors.[1–6] Although batteries are currently the most mature energy-storage devices, they apparently have several limitations especially for wearable applications, including potential safety risks, short cycle life, rather long charging time, and rigid requirement for form factors.[4,7] In the meantime, planar supercapacitors have emerged as favorable alternatives or complements to batteries with the desirable attributes of higher power density, fast charge/discharge, better operation safety, longer cycling life, and high compatibility with flexible, diverse, and miniaturized form factors.[7–11] In addition, the in-plane interdigitated electrode configuration with separator-free design is preferable for integration with microelectronic systems and enables further miniaturization of portable and wearable devices.[8,12–15] Although techniques including photolithography and laser scribing have commonly been used for planar supercapacitor fabrication in the past,[2,16–21] their relatively high cost and/or low throughput pose challenges for scalable device fabrication. In recent years, the inkjet-printing method, which enables scalable and feasible fabrication without rigid operation requirements,[22,23] has triggered increasing research interest on fabrication of various functional electronic devices such as transistors,[24–26] photodetectors,[27] and light-emitting diodes (LEDs).[28]

Herein, we demonstrated a printing method to construct all-solid-state planar supercapacitors on flexible substrates. In such devices, the pattern of interdigitated metal finger arrays was inkjet printed on flexible substrates. Additionally, the hierarchical nickel (Ni)@manganese dioxide (MnO_2) nanocoral structures were then uniformly formed on the interdigitated finger arrays by facile electrochemical deposition to significantly enhance pseudocapacitive performance, and at the same time to reduce the interspace between finger electrodes down to 5 μm. Based on such unique hierarchical Ni@MnO_2 nanostructures and high electrode density, the as-built planar supercapacitor rendered a largely enhanced areal capacitance of 47.3 mF cm^{-2} at a current density of 0.54 mA cm^{-2} and 52.9 mF cm^{-2} at the scan rate of 5 mV s^{-1}, which is 2.5 times of that without nanocoral structure, and such capacitance is even comparable with supercapacitors in stacked configuration.[29,30] Meanwhile, the device exhibited the highest specific power of 39.6 W cm^{-3} and the specific energy of 11.1 mWh cm^{-3}. More interestingly, due to utilization of inkjet-printing technique, excellent versatility on electrode-pattern artistic design has been achieved. Particularly, working supercapacitors with artistically designed patterns are demonstrated here, and they have been used to drive LEDs. To further demonstrate the scalability of the developed approach here, "power papers" with design versatility were fabricated, which are large planar supercapacitor with a device area of up to 100 cm^2. These "power papers" were successfully assembled together to provide energy for a self-powered wearable system. Overall, the printable method reported here opens up opportunities for facile and scalable fabrication of energy devices with excellent versatility. These energy devices can be broadly used in future wearable components.

The process of printable fabrication of planar supercapacitor is schematically shown in **Figure 1** with details provided in the "Experimental Section". Briefly, the interdigitated finger electrode arrays were inkjet printed with silver (Ag) nanoparticle

Dr. Y. Lin, Dr. Y. Gao, Prof. Z. Y. Fan
Department of Electronic and Computer Engineering
The Hong Kong University of Science and Technology
Clear Water Bay, Kowloon, Hong Kong, SAR China
E-mail: eezfan@ust.hk

DOI: 10.1002/adma.201701736

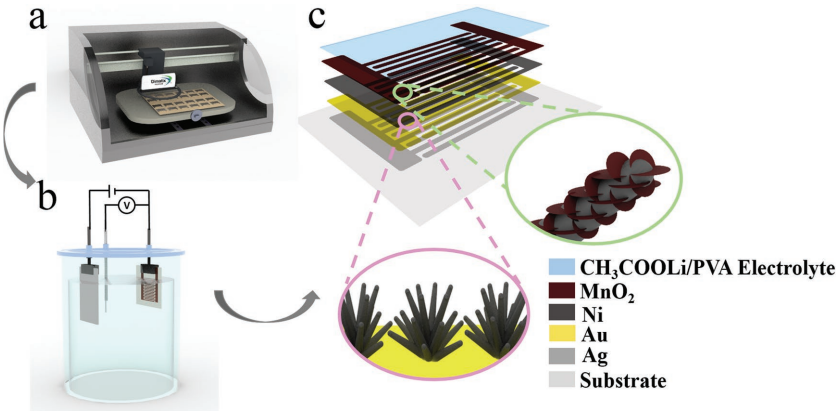

Figure 1. Schematic illustration of the printable fabrication procedure. a) Interdigitated electrode patterns were inkjet printed onto the flexible PET-based substrate. b) Three-step electrochemical deposition. c) The as-fabricated all-solid-state planar supercapacitor with hierarchical Ni@MnO_2 nanocoral nanostructures.

colloidal ink onto the porous poly(ethylene terephthalate) (PET) substrate (Figure 1a), followed by a three-step electrochemical deposition (Figure 1b). First, a thin layer of gold (Au) with fine roughness was deposited on the Ag electrodes. Then unique Ni nanocoral structures were deposited on Au by overpotential electrochemical deposition. Afterward, pseudocapacitive MnO_2 nanoflakes were conformally deposited on the surface of Ni dendrites to achieve Ni@MnO_2 hierarchical electrodes with large surface area. To realize all-solid-state supercapacitors that can be easily embedded as energy-storage devices onto portable and wearable devices, 1 M lithium acetate/poly(vinyl acetate) (CH_3COOLi/PVA) gel was utilized as electrolyte and drop-cast onto the surface of interdigitated electrodes (Figure 1c).

The scanning electron microscopy (SEM) images of the electrode morphologies corresponding to each fabrication steps are shown in **Figure 2**. Figure 2a shows a printed Ag finger array consist of interdigitated electrodes with the width of ≈25 µm and the minimized interspace between neighboring fingers in the range of 8–12 µm. Note that such pattern resolution is comparable with that can be achieved via conventional photolithography technique. However, the printable fabrication is apparently much more cost effective and scalable than photolithography. The Au layer with fine roughness deposited on a Ag pattern (Figure 2b) can be realized by controlling the applied voltage during Au electrochemical deposition, and Ni nanocoral structures with an average length of 3.5 µm are distributed uniformly on the Au layer (Figure 2c,d). It is worth mentioning that the small grains on the Au thin film can serve as the nucleation sites for the uniform growth of Ni nanocoral structures, compared with the nanostructures deposited directly on the Ag layer (Figure S1, Supporting Information). Moreover, the ductility of the Au film is favorable to stabilize the nanocoral structures and reduces the potential risk of forming cracks on Ni structures that leads to device failure (Figure S1b, Supporting Information). Thus, the deposition of a thin layer of Au with fine roughness is essential for good yields of high-performance devices. After Ni nanocoral formation, the interspaces between neighboring finger electrodes can be further narrowed down to an average of 5 µm, and such a short distance between electrodes enables rapid ion transport and diffusion to realize high power capability.[31] Technically, it is also the optimized fabrication form factor to prevent shorting-contact between neighboring electrodes and maintain a considerate device yield rate. Note that the formation of Ni nanocoral structure is realized

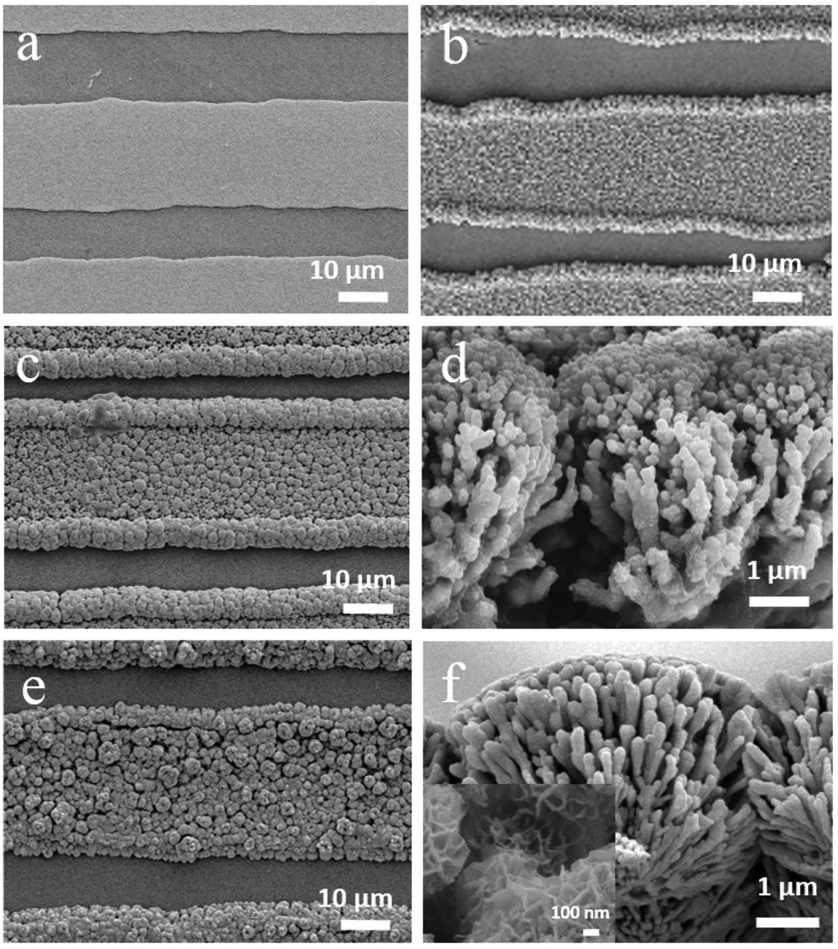

Figure 2. SEM images of nanocoral-structured electrodes. a) Inkjet-printed Ag pattern. b) Au layer with fine roughness deposited on Ag pattern. c,d) Ni nanocoral. e,f) MnO_2 nanoflakes on Ni nanocoral (Ni@MnO_2). Parts (c) and (e) are low-magnification top-view images and parts (d) and (f) and the inset are high-magnification images.

via overpotential electrochemical deposition with appropriate electrolyte composition in room temperature, and hydrogen evolution can be observed during the process. On the contrary, planar Ni film can be achieved when a low voltage is applied for deposition (Figure S2a,b, Supporting Information). From a classic nucleation theory's point of view, such an electrochemical deposition process is a cooperative effect of several factors such as overpotential, surface energy reduction, hydrogen evolution, and ion diffusion.[5,15,32–37] Here, based on the phenomenon and morphology evolution observed during deposition process (Figure S3, Supporting Information), and referring to previous theoretical studies on formation mechanism of nanostructure, we proposed that the formation of such unique Ni nanocorals on Au layer mainly consists of three important steps: i) by applying an periodic negative overpotential, the Ni^{2+} ions are rapidly driven to the working electrode and reduced at the Au/electrolyte interface to form Ni nuclei. The nucleation of Ni nuclei is promoted by overpotential and the resulting Ni particles are capable of serving as growth centers for nanostructure formation;[5,35] ii) guided by surface energy reduction, surface with higher energy is favorable for atom attachment. Such oriented aggregation primarily follows one direction and gradually forms the branch-like structure;[5,33,35] and iii) the reduction of Ni is accompanied by hydrogen evolution and generates large amount of bubbles that serve as dynamic template to assist the formation of such a nanocoral structure.[38–40] Here, MnO_2 nanoflakes were used as pseudocapacitive active materials, and they were uniformly deposited on the surface of Ni nanocoral, as shown in Figure 2e,f. To further investigate the surface properties of the as-fabricated Ni@MnO_2 nanocoral electrodes on PET-based substrates, Brunauer–Emmett–Teller (BET) analysis was performed on adsorption–desorption isotherms (Figure S4a, Supporting Information). Since the mass of electrode materials is negligible compared with the weight of the substrates, a blank and planar PET-based substrate was employed for comparison. The as-fabricated hierarchical Ni@MnO_2 nanocoral structures on PET substrates provide a BET surface area of 34.9 $m^2\ g^{-1}$, which realizes a remarkable enhancement of surface area over 250% than 9.7 $m^2\ g^{-1}$ of the blank PET planar substrates. Using the Barrett–Joyner–Halenda (BJH) model, the pore size distribution of such Ni@MnO_2 nanocoral structures mainly center around 20 nm (Figure S4b, Supporting Information), which matches with the SEM image (inset of Figure 2f). Such mesoporous structures with large surface area promote the electrochemical reactions. Meanwhile, the minimized interspace enables effective utilization of device area and shortens the electrolyte ion travel path. All of these advantages are key factors contributing to the significantly enhanced device performance of the assembled devices which will be discussed further later.

The material composition distribution for the Ni@MnO_2 electrode was probed by an energy dispersive spectrometer (EDS) (Figure S5, Supporting Information) and Mn^{4+} ion was indicated in X-ray photoelectron spectroscopy (Figure S6, Supporting Information). The crystal structure of the as-fabricated hierarchical electrodes was characterized by X-ray diffraction (XRD) (Figure S7, Supporting Information). The well-crystallized Ni can be indicated by the strong and narrow peaks at scattering angles of 44.54°, 51.86°, and 76.64°, corresponding to the crystal planes of (111), (200), and (220), respectively, which index the face-centered cubic structure of crystalline Ni.[35,38] Besides, the peaks from Au and substrate that contains silicon dioxide (SiO_2) can be identified in the spectrum.

It is worth mentioning that for a planar supercapacitor, the areal capacitance is considered as the more important figure-of-merit than volumetric/gravimetric capacitance.[2,7] Therefore, we have performed systematic experiments to optimize the areal capacitance of micro-supercapacitor devices. In general, active material mass loading, i.e., MnO_2, largely determines the overall capacitance of the device. On one hand, adequate amount of MnO_2 is essential for energy storage. On the other hand, with excessive MnO_2 mass loading, the electrical conductivity decreases and ion transportation can be hindered. Therefore, optimization of active material mass loading was first investigated in this work. Typically, the controllable deposition of MnO_2 was achieved by applying a periodic voltage pulse with different cycles, and the number of cycles determines the amount of MnO_2 layer thickness/mass loading (SEM images shown in Figure S8, Supporting Information). Generally, the capacitance is expected to increase with more MnO_2 for redox reaction. However, the overloaded MnO_2 tends to form a denser layer, and electron transfer between MnO_2 and Ni nanocoral current collectors will be hindered, as shown in Figure S8e,f (Supporting Information). Moreover, the porosity of nanocoral structure will largely decrease and that leads to less surface contact area with the ion in electrolyte and uncompleted electrochemical reaction. Therefore, the device capacitance eventually decreased with excessive MnO_2 deposition. To evaluate the electrochemical performance of the as-fabricated flexible all-solid-state planar supercapacitors, cyclic voltammetry (CV) measurements at a scan rate from 5 to 100 mV s^{-1} were tested, together with galvanostatic charging–discharging (GCD) measurements at a current density from 0.54 to 2.16 mA cm^{-2}, with a voltage range from 0 to 0.8 V. The corresponding CV curves of the devices with different MnO_2 loading mass are shown in **Figure 3**a and Figure S9 (Supporting Information). It is obviously indicated from the CV curves that the device achieves the highest areal capacitance after 25 cycles MnO_2 deposition (Figure 3a,b), in this case, a uniform layer of MnO_2 with a thickness of 100 nm was conformally deposited on the nanostructured electrodes (Figure S8d, Supporting Information). The optimized device performance is also indicated both by the quasi-rectangular CV curves with negligible shape distortion at the increasing scan rate (Figure 3c) and the GCD curves with close to linear voltage–time profile exhibiting a high Coulombic efficiency over 80% (Figure 3d). The highest areal capacitance achieved is 52.7 mF cm^{-2} at the scan rate of 5 mV s^{-1} and 47.3 mF cm^{-2} at the discharging current density of 0.54 mA cm^{-2}. And such respectable values are among the highest when compared with previous reports on planar supercapacitors.[7,16,31,41–43] Also, the areal capacitance still maintains 58% at 100 mV s^{-1} and 63% at 2.16 mA cm^{-2} (Figure 3e), indicating its remarkable rate capability. Besides, the stability of such a device was demonstrated by the cyclic life test conducted at the scan rate of 100 mV s^{-1} (Figure 3f). The capacitance degradation was mainly observed during the initial cycles, and afterward, the capacitance tends to be stable and maintains over 80% of its capacitance after 5000 cycle test. The capacitance decay tendency during the long-term cycling test could be attributed to the following factors:

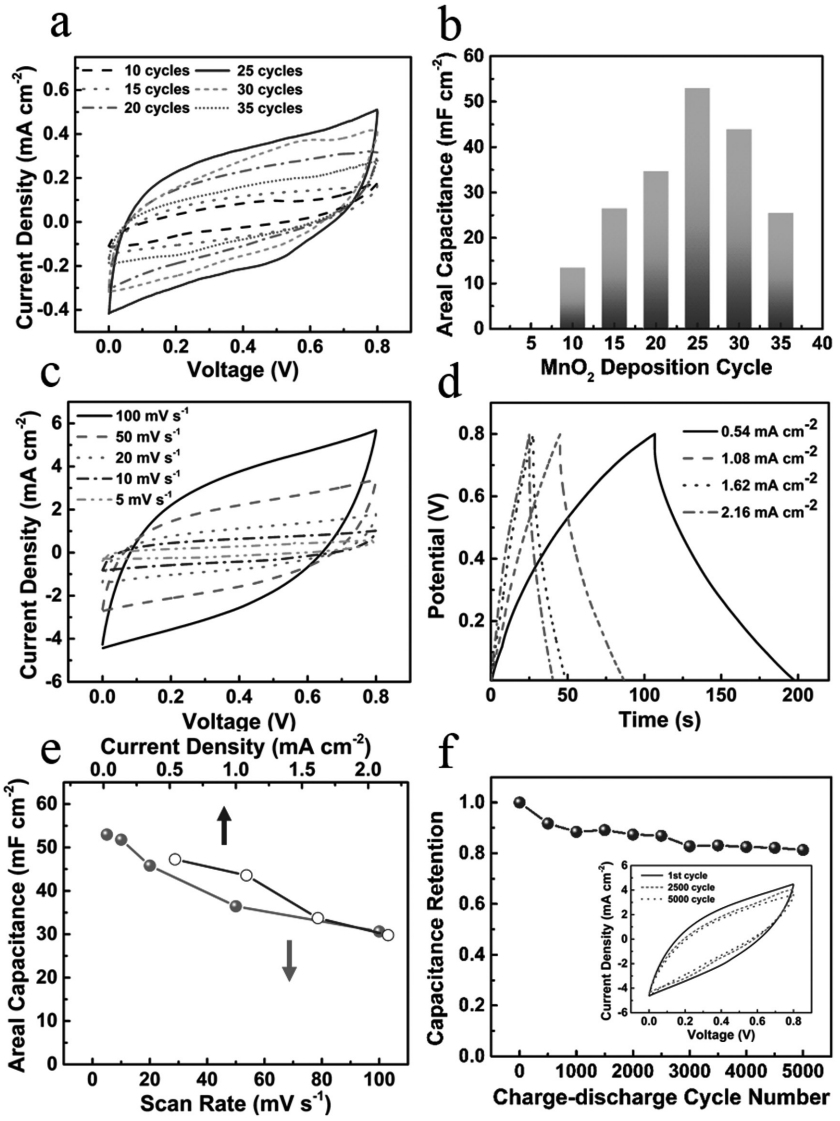

Figure 3. Electrochemical measurements of Ni@MnO_2 nanocoral-structured planar supercapacitors. a) CV curves of devices with different number of MnO_2 deposition cycles recorded at scan rates of 5 mV s^{-1}. b) Areal capacitance of devices with different number of MnO_2 deposition cycles. c) CV curves of the device with optimized MnO_2 mass loading (25 deposition cycles) recorded at scan rates of 5, 10, 20, 50, and 100 mV s^{-1}. d) GCD curves of the device with optimized MnO_2 mass loading at a discharge current of 0.54, 1.08, 1.62, and 2.16 mA cm^{-2}. e) Areal capacitances of device with optimized MnO_2 mass loading calculated from CV and GCD measurements, respectively. f) The cycling stability test of the device at a scan rate of 100 mV s^{-1}. Inset: CV curves at the first cycle, after 2500 and 5000 cycles.

i) volume expansion of active material can be introduced by intercalation of electrolyte ion into the bulk material during the redox reaction,[30,44] and thus, dissolution of MnO_2 into the electrolyte might be the main reason for the initial capacitance degradation until the equilibrium state established between dissolution and re-deposition; ii) degradation of active material might occur after cycles of dissolution and re-deposition;[1] and iii) the vaporization of electrolyte solvent in ambient environment would hinder the ion transportation.

To further confirm the performance enhancement by using the unique hierarchical nanocoral-structured electrodes, supercapacitors with Ni@MnO_2 planar electrodes were fabricated for the sake of comparison (Figure S2c, Supporting Information). MnO_2 was also deposited on the planar interdigitated electrodes with the same deposition cycles. As shown in **Figure 4**a, the device with nanocoral-structured electrode shows a CV curve with much larger enclosed area and more symmetric rectangular shape. Remarkable capacitance enhancement of over 150% at the low scan rate of 5 mV s^{-1} and over 300% at 100 mV s^{-1} can be obtained by using the nanocoral structure. Such results are also consistent with the BET surface area enhancement and demonstrate the improvement on rate capability (Figure 4b). Specifically, this performance enhancement can be attributed to two reasons: i) with the same mass loading, the larger surface area of nanocoral structures enables the formation of a thinner layer of MnO_2, hence facilitating the electron transport;[45,46] ii) the hierarchical nanocoral structure allows fast ion diffusion alongside the active material and provides adequate electrochemical site for ion landing, leading to a completed electrochemical reaction to enhance the energy-storage capability.[15,47–49]

The interspace between finger electrodes is another pivotal factor that affects the normalized capacitance and the electrochemical performance.[13] Given the same footprint area, minimizing the interspace allows higher density of finger electrodes and maximizing the effective device area for electrochemical reaction. In addition, the ionic diffusion pathway is also shorter with smaller electrode interspace. Therefore, the normalized areal capacitance is anticipated to be largely enhanced. To conduct a systematic study, devices with the finger width of 35 μm and interspaces of 5 μm (W35G5), 25 μm (W35G25), and 65 μm (W35G65) were fabricated (Figure S10a–c, Supporting Information) and characterized (Figure 4c; Figure S11a,b, Supporting Information). The corresponding device areas/volumes and areal/volumetric capacitances are also calculated (Figure 4d and Figure S10 and S11c,d, Supporting Information). The areal capacitance of the device with an interspace of 5 μm is over 60% and 170% higher than that of the devices with 25 and 65 μm interspaces, respectively (Figure 4d). Apart from the normalized areal capacitance, the electrochemical impedance spectroscopy (EIS) measurements with the frequency ranges from 100 kHz to 0.01 Hz were also carried out to prove the benefit of minimizing the electrode interspace. As shown in Figure 4e, the largest radius of the semicircle in the high-frequency region indicates that the device with 65 μm interspace has the largest charge transfer impedance, resulted

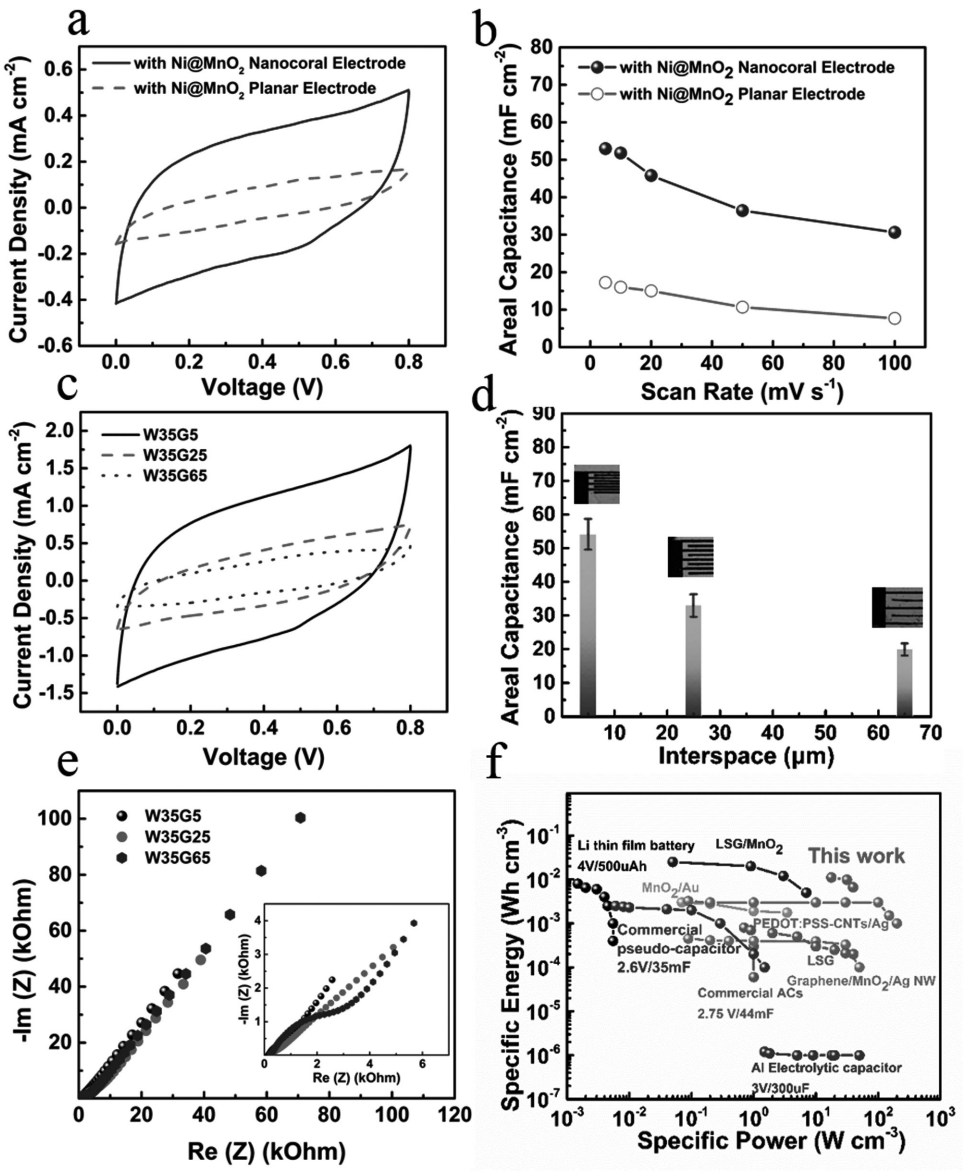

Figure 4. Performance enhancement of the planar supercapacitor with hierarchical Ni@MnO_2 nanocoral-structured electrode with minimized finger interspace. a) CV curves of devices with Ni nanocoral and Ni film as current collectors recorded at a scan rate of 5 mV s^{-1}. b) Areal capacitance of devices with Ni nanocoral and Ni film as current collectors. c) CV curves of devices with an electrode finger width of 35 μm and finger interspaces of 5 μm (W35G5), 25 μm (W35G25), and 65 μm (W35G65) recorded at a scan rate of 20 mV s^{-1}. d) Areal capacitance of devices W35G5, W35G25, and W35G65. Inset: optical microscopy images of devices. e) EIS Nyquist plots of devices W35G5, W35G25, and W35G65 at frequencies ranging from 100 kHz to 0.01 Hz. Inset: the enlarged high-frequency range. f) Ragone plots show the specific energy and power of the device, in comparison to the other energy-storage devices.

from the long ion diffusion distance between the coupled electrodes. As the devices had the same number of electrodes, the direct-current (DC) resistances was all around 40 Ω at the high-frequency region.

The specific energy and specific power of the as-fabricated flexible planar supercapacitor are compared with commercial products and the relevant works, as shown in the Ragone plot (Figure 4f). The device with hierarchical Ni@MnO_2 nanocoral electrodes exhibits a highest specific energy of 11.1 mW h cm^{-3}, which is quite competitive when compared with several reported works in fields of planar supercapacitors, and demonstrates 3.7 times higher than the reported poly(3,4-ethylenedioxythiophene):poly(styrene sulfonate) (PEDOT:PSS)-carbon nanotubes (CNTs)/Ag-based supercapacitor fabricated via the inkjet-printing method,[42] 40 times higher than that of laser-scribed graphene (LSG) supercapacitor,[16] 30 times higher than that of a graphene/MnO_2/Ag nanowire supercapacitor,[31] and four orders of magnitude improvement than that of aluminum electrolytic capacitors (3 V/300 μF). The highest specific power achieved by the device is 39.6 W cm^{-3}, which is four orders of magnitude higher than that of the reported commercial lithium thin-film battery (4 V/500 μA h). Moreover, the

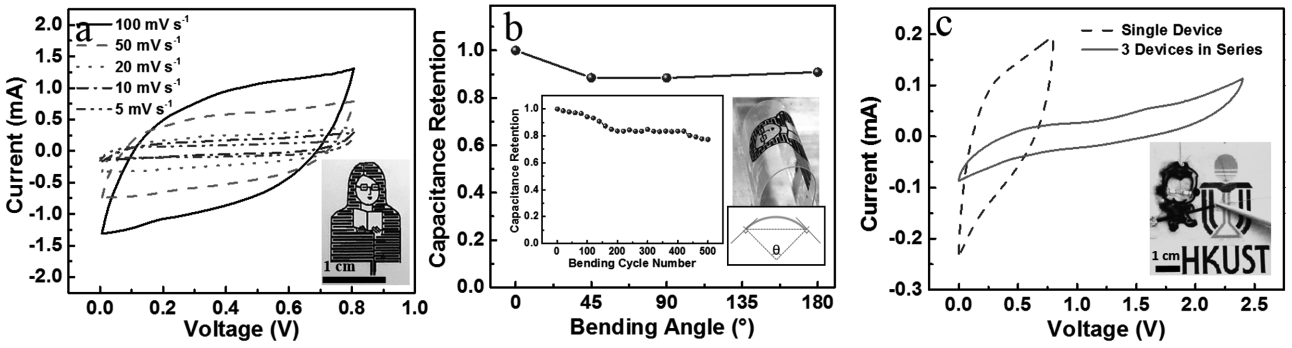

Figure 5. Photos and characterization of planar supercapacitors with artistic designs. a) CV curves of supercapacitor with the pattern of a portrait recorded at scan rates of 5, 10, 20, 50, and 100 mV s^{-1}. Inset: photograph of the device. b) The bending stability test of supercapacitor. Inset: bending cycle stability and the photo of device bended with 180°. c) CV curves of single unit and three units in series of the "Monkey King" tandem supercapacitor. Inset: photograph of the "Monkey King" tandem supercapacitor powers up a pair of LEDs.

as-fabricated planar nanocoral supercapacitors have a highly enhanced energy-storage capability compared with commercial activated carbon-based supercapacitors (2.75 V/44 mF) and commercial pseudocapacitor (2.6 V/35 mF).

For application in wearable electronics, the flexibility on the active and passive device design is highly preferred. In this regard, inkjet printing is arguably the most versatile and cost-effective method to achieve device artistic design without relying on any mask. Particularly in this work, with the maskless printable method, supercapacitors with various artistic pattern designs were successfully fabricated using the nanocoral electrodes. **Figure 5**a shows a supercapacitor with the pattern of a portrait that delivers a capacitance of 72.5 mF at a scan rate of 5 mV s^{-1}. The detailed electrode-pattern design can be found in Figure S12 (Supporting Information). The excellent flexibility of the device is demonstrated in Figure 5b. Notably, the device retained 90.8% capacitance of the initial value under a bending angle of 180° and a capacitance retention of 77.4% was achieved after 500 cycles under 180° bending angle (the inset of Figure 5b). Beyond the aesthetic property, various device configurations at the circuit level can be conveniently achieved for practical applications. To verify such a concept, three supercapacitors in series connection were integrated into a "Monkey King" pattern as shown in Figure 5c. And this device can be successfully charged up to 2.4 V without showing an oxygen evolution redox peak. To demonstrate the functionality of this device, a pair of LEDs, symbolizing the red eyes of "Monkey King," were powered up by such a tandem supercapacitor (the inset of Figure 5c and Movie S1, Supporting Information).

The printable method also enables large-scale fabrication on a variety of flexible substrates. Such scalability and feasibility were first demonstrated by fabrication of a large-scale supercapacitor, in size of 10 cm × 10 cm, on a commercial glossy paper (Figure S13a, Supporting Information). The as-fabricated 100 cm^2 "power paper" consisted of 25 pairs of interdigitated electrodes with both electrode width and interspace of 1 mm. Furthermore, large-sized tandem supercapacitors in the patterns of two logos of Hong Kong University of Science and Technology (HKUST), both consist of four supercapacitors in series connection, were constructed (Figure S13b,c, Supporting Information) and can be charged up to 3.2 V. Additionally, a self-powered T-shirt was made with the two artistic tandem supercapacitors connected in series, serving as the energy-storage module and collecting the energy generated by the commercial polycrystalline silicon solar cell panels (Figure S13d, Supporting Information). The three letters of "UST", as the energy-consuming part, consists of 41 LEDs in parallel connection with purple, white, and blue colors. Under room light illumination, the LEDs can be directly powered up by solar cell panels (**Figure 6**a,b), while in the dark condition, the LED arrays can be lighted up by the energy released from the supercapacitors (Figure 6c,d; Movie S2, Supporting Information). Such a self-powered system as a proof of concept clearly demonstrates the excellent performance of the printed supercapacitors, their versatility on device design, and promising potency for future broad wearable applications.

Here, we demonstrate scalable and printable fabrication of interdigitated electrodes for flexible supercapacitors. In conjunction with facile electrochemical deposition, unique hierarchical Ni@MnO_2 nanocoral structures were deposited on the electrodes with high density, thus drastically improved the supercapacitor device performance. Owing to the flexible and versatile inkjet-printing pattern designs, artistic designed supercapacitors were fabricated. The devices also displayed desirable attributes of flexibility, electrochemical stability, and attractive form factors. Moreover, large-scale artistic supercapacitors were successfully fabricated and integrated into a wearable self-powered system, which further demonstrates their promising potency as energy-storage devices for future portable and wearable devices.

Experimental Section

Fabrication of Planar Supercapacitor Pattern: The patterns with interdigitated electrode fingers were first designed in computer painting program and then imported to the software of Dimatrix Material Printer (DMP 2831, FUJIFILM). The pattern was then printed on PET-based substrate (Novele IJ-220, NovaCentrix) or glossy paper (CG851A, HP) with Ag ink (Metalon JS-B25HV, NovaCentrix) and annealed at 60 °C for 30 min to evaporate the solvent.

Fabrication of Ni@MnO_2 Nanocoral-Structured Electrodes and Ni@MnO_2 Planar Electrodes: All the chemicals were of analytical grade. The hierarchical nanocoral-structured electrodes were fabricated in a three-step electrochemical deposition process. The electrochemical depositions were conducted in a three-electrode configuration using a

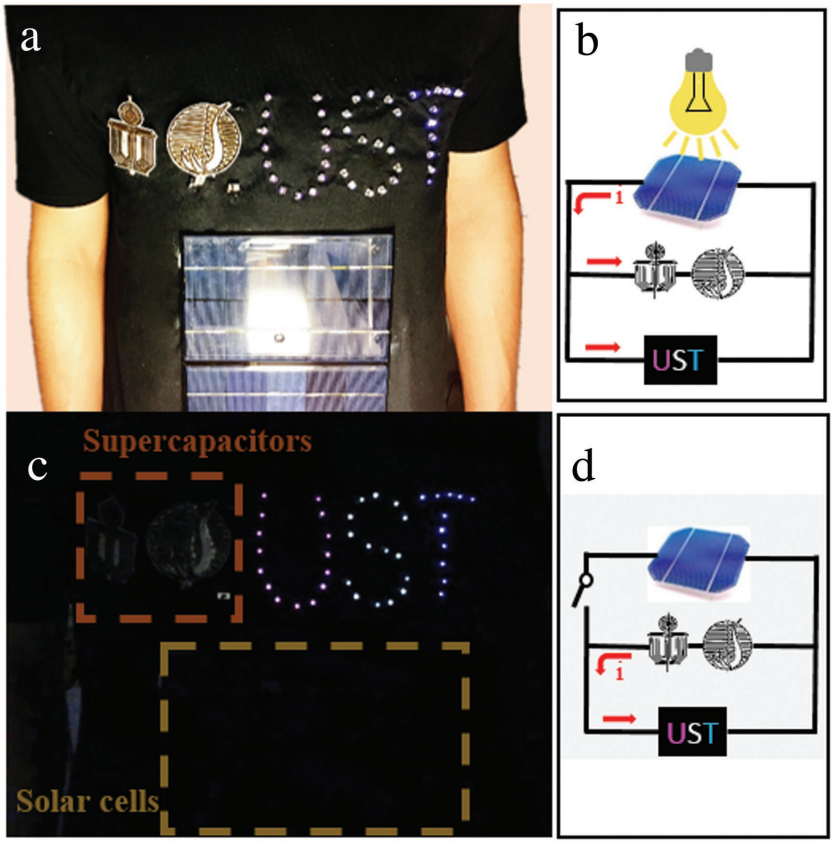

Figure 6. A wearable self-powered system on T-shirt consisting of solar cell panels, artistic designed supercapacitors, and an LED array could be lit up by: a,b) solar cell panels under illumination with schematic circuit diagrams shown in part (b), or by c,d) supercapacitors under dark conditions with schematic circuit diagrams shown in part (d).

potentiostat (SG 300, Gamry Instruments). Au deposition was conducted by applying a periodic voltage wave with an amplitude of –0.8 V, a frequency of 10 Hz, and a duty cycle of 50% in gold plating solution (Elevate Gold 7990, Technic, Inc., USA) for 1500 cycles, leading to the formation of around 100 nm slightly porous Au film. The electrolyte for Ni deposition was prepared by dissolving 30 g of nickel(II) sulfate hexahydrate ($NiSO_4{\cdot}6H_2O$), 4.5 g of nickel(II) chloride hexahydrate ($NiCl_2{\cdot}6H_2O$), and 4.5 g of boric acid (H_3BO_3) in 100 mL deionized (DI) water under vigorous stirring. Ni nanocoral with an average thickness of 3.5 µm was synthesized under a periodic voltage wave with an amplitude of –2 V, a frequency of 10 Hz, a duty cycle of 50% for 2500 cycles. Note that the growth rate of Ni nanocoral was slightly higher along the margin of patterns. For comparison, the planar Ni film was also fabricated via the similar method under a periodic voltage wave with amplitude of –1 V. The MnO_2 deposition solution includes 0.05 M manganese acetate ($Mn(CH_3COO)_2$), 0.05 M sodium sulfate (Na_2SO_4), and 10% ethanol. A periodic voltage wave of 10% duty cycle, an upper voltage of 1.5 V, 90% of 0.7 V, and a frequency of 0.1 Hz were applied.

Assembling of All-Solid-State Planar Supercapacitors: About 12 g of PVA and 12 g of 85 wt % CH_3COOLi were dissolved in 120 mL DI water. After that, the solution was vigorously stirred at 85 °C until it became clear. Then, the solution was cooled down to room temperature and used as a gel electrolyte. The electrolyte was drop-cast on the interdigitated electrodes and was kept in air for 24 h to make it an all-solid-state planar supercapacitor.

Characterization and Measurements: Various analytical techniques were utilized to characterize the as-fabricated nanostructured electrodes and the as-fabricated supercapacitors. Morphologies were characterized using field-emission scanning electron microscopy (JSM-7100F, Japan). Nitrogen adsorption isotherms were measured with a Micromeritics ASAP 2020 sorptometer. Specific surface area was determined with BET equation, and the distribution of pore size was calculated from the desorption curve by the BJH method. Chemical compositions were studied by EDS (JSM-7100F, Japan) and X-ray photoelectron spectroscopy (PHI 5600, USA), and the crystal structure by XRD (Bruker D8 X-ray Diffractometer, USA). CV measurements based on a two-electrode configurations were performed on an electrochemical workstation (CHI 660E, China) at different scan rates of 5, 10, 20, 50, and 100 mV s^{-1}. GCD and EIS measurements based on a two-electrode configuration were performed on an electrochemical workstation (Gamry Instruments, USA). GCD was measured at 0.54, 1.08, 1.62, and 2.16 mA cm^{-2}. EIS was measured with the frequency ranges from 100 kHz to 0.01 Hz with a potential amplitude of 10 mV. Calculations of the areal capacitance and specific power and energy are discussed in detail in the Supporting Information.

Supporting Information

Supporting Information is available from the Wiley Online Library or from the author.

Acknowledgements

The authors thank Y. Zhang and Alex H. K. Wong from Materials Characterization and Preparation Facility (MCPF), The Hong Kong University of Science and Technology for their help on SEM analysis. This work was supported by General Research Fund (16237816) from Hong Kong Research Grant Council,ITS/362/14FP from Hong Kong Innovation Technology Commission and National Natural Science Foundation of China (project 51672231). The authors also acknowledge the support from Center for 1D/2D Quantum Materials and State Key Laboratory on Advanced Displays and Optoelectronics at HKUST.

Note: The Experimental Section, *Fabrication of Ni@MnO_2 Nanocoral-Structured Electrodes and Ni@MnO_2 Planar Electrodes*, was updated on November 14, 2017. This clarifies that 4.5 g of boric acid was used to prepare the electrolyte.

Conflict of Interest

The authors declare no conflict of interest.

Keywords

flexible devices, inkjet printing, nanocoral structures, planar supercapacitors, wearable self-powered systems

Received: March 28, 2017
Revised: June 3, 2017
Published online: October 5, 2017

[1] P. Simon, Y. Gogotsi, *Nat. Mater.* **2008**, *7*, 845.
[2] M. R. Lukatskaya, B. Dunn, Y. Gogotsi, *Nat. Commun.* **2016**, *7*, 12647.
[3] Z. L. Wang, *Nano Today* **2010**, *5*, 512.

[4] L. Li, Z. Wu, S. Yuan, X. Zhang, *Energy Environ. Sci.* **2014**, *7*, 2101.
[5] Z. An, J. Zhang, S. Pan, *CrystEngComm* **2010**, *12*, 500.
[6] S. Shi, C. Xu, C. Yang, Y. Chen, J. Liu, F. Kang, *Sci. Rep.* **2013**, *3*, 2598.
[7] N. A. Kyeremateng, T. Brousse, D. Pech, *Nat. Nanotechnol.* **2017**, *12*, 7.
[8] L. Li, Z. Lou, W. Han, D. Chen, K. Jiang, G. Shen, *Adv. Mater. Technol.* **2017**, *2*, 1600282.
[9] G. Yu, X. Xie, L. Pan, Z. Bao, Y. Cui, *Nano Energy* **2013**, *2*, 213.
[10] H. Hu, Z. Pei, H. Fan, C. Ye, *Small* **2016**, *12*, 3059.
[11] Z. Zhang, L. Wang, Y. Li, Y. Wang, J. Zhang, G. Guan, Z. Pan, G. Zheng, H. Peng, *Adv. Energy Mater.* **2017**, *7*, 1601814.
[12] J. Lin, C. Zhang, Z. Yan, Y. Zhu, Z. Peng, R. H. Hauge, D. Natelson, J. M. Tour, *Nano Lett.* **2012**, *13*, 72.
[13] T. M. Dinh, K. Armstrong, D. Guay, D. Pech, *J. Mater. Chem. A* **2014**, *2*, 7170.
[14] P. Chen, J. Yang, S. Li, Z. Wang, T. Xiao, Y. Qian, S. Yu, *Nano Energy* **2013**, *2*, 249.
[15] T. Nguyen, S. Eugénio, M. Boudard, L. Rapenne, M. J. Carmezim, T. M. Silva, M. F. Montemor, *Nanoscale* **2015**, *7*, 12452.
[16] M. F. El-Kady, R. B. Kaner, *Nat. Commun.* **2013**, *4*, 1475.
[17] H. Huang, C. Chung, C. Hsieh, P. Kuo, H. Teng, *Nano Energy* **2016**, *21*, 90.
[18] M. Beidaghi, C. Wang, *Adv. Funct. Mater.* **2012**, *22*, 4501.
[19] J. Cai, C. Lv, A. Watanabe, *J. Mater. Chem. A* **2016**, *4*, 1671.
[20] W. Gao, N. Singh, L. Song, Z. Liu, A. L. M. Reddy, L. Ci, R. Vajtai, Q. Zhang, B. Wei, P. M. Ajayan, *Nat. Nanotechnol.* **2011**, *6*, 496.
[21] R. Li, R. Peng, K. Kihm, S. Bai, D. Bridges, U. Tumuluri, Z. Wu, T. Zhang, G. Compagnini, Z. Feng, *Energy Environ. Sci.* **2016**, *9*, 1458.
[22] K. Chen, W. Gao, S. Emaminejad, D. Kiriya, H. Ota, H. Y. Y. Nyein, K. Takei, A. Javey, *Adv. Mater.* **2016**, *28*, 4397.
[23] Z. Yin, Y. Huang, N. Bu, X. Wang, Y. Xiong, *Chin. Sci. Bull.* **2010**, *55*, 3383.
[24] H. Sirringhaus, T. Kawase, R. H. Friend, T. Shimoda, M. Inbasekaran, W. Wu, E. P. Woo, *Science* **2000**, *290*, 2123.
[25] F. Torrisi, T. Hasan, W. Wu, Z. Sun, A. Lombardo, T. S. Kulmala, G. Hsieh, S. Jung, F. Bonaccorso, P. J. Paul, *ACS Nano* **2012**, *6*, 2992.
[26] P. H. Lau, K. Takei, C. Wang, Y. Ju, J. Kim, Z. Yu, T. Takahashi, G. Cho, A. Javey, *Nano Lett.* **2013**, *13*, 3864.
[27] X. Liu, L. Gu, Q. Zhang, J. Wu, Y. Long, Z. Fan, *Nat. Commun.* **2014**, *5*, 4007.
[28] S. Chang, J. Liu, J. Bharathan, Y. Yang, J. Onohara, J. Kido, *Adv. Mater.* **1999**, *11*, 734.
[29] Y. Gao, H. Jin, Q. Lin, X. Li, M. M. Tavakoli, S. Leung, W. M. Tang, L. Zhou, H. L. W. Chan, Z. Fan, *J. Mater. Chem. A* **2015**, *3*, 10199.
[30] Y. Gao, Y. Lin, J. Chen, Q. Lin, Y. Wu, W. Su, W. Wang, Z. Fan, *Nanoscale* **2016**, *8*, 13280.
[31] W. Liu, C. Lu, X. Wang, R. Y. Tay, B. K. Tay, *ACS Nano* **2015**, *9*, 1528.
[32] A. Pei, G. Zheng, F. Shi, Y. Li, Y. Cui, *Nano Lett.* **2017**. *17*, 1132.
[33] J. K. Lee, Y. Yi, H. J. Lee, S. Uhm, J. Lee, *Catal. Today* **2009**, *146*, 188.
[34] J. Ji, P. Li, S. Sang, W. Zhang, Z. Zhou, X. Yang, H. Dong, G. Li, J. Hu, *AIP Adv.* **2014**, *4*, 031329.
[35] J. Wang, L. Wei, L. Zhang, Y. Zhang, C. Jiang, *CrystEngComm* **2012**, *14*, 1629.
[36] Z. Sun, S. Firdoz, E. Y. Yap, L. Li, X. Lu, *Nanoscale* **2013**, *5*, 4379.
[37] S. Morin, A. Lachenwitzer, O. Magnussen, R. Behm, *Phys. Rev. Lett.* **1999**, *83*, 5066.
[38] X. Xia, J. Tu, Y. Zhang, Y. Mai, X. Wang, C. Gu, X. Zhao, *J. Phys. Chem. C* **2011**, *115*, 22662.
[39] H. C. Shin, J. Dong, M. Liu. *Adv. Mater.* **2003**, *15*, 1610.
[40] Y. Li, Y. Song, C. Yang, X. Xia. *Electrochem. Commun.* **2007**, *9*, 981
[41] W. Si, C. Yan, Y. Chen, S. Oswald, L. Han, O. G. Schmidt, *Energy Environ. Sci.* **2013**, *6*, 3218.
[42] W. Liu, C. Lu, H. Li, R. Y. Tay, L. Sun, X. Wang, W. L. Chow, X. Wang, B. K. Tay, Z. Chen, J. Yan, K. Feng, G. Lui, R. Tjandra, L. Rasenthiram, G. Chiu, A. Yu, *J. Mater. Chem. A* **2016**, *4*, 3754.
[43] M. F. El-Kady, M. Ihns, M. Li, J. Y. Hwang, M. F. Mousavi, L. Chaney, A. T. Lech, R. B. Kaner, *Proc. Natl. Acad. Sci. USA* **2015**, *112*, 4233.
[44] H. Zhao, C. Wang, R. Vellacheri, M. Zhou, Y. Xu, Q. Fu, M. Wu, F. Grote, Y. Lei. *Adv. Mater.* **2014**, *26*, 7654.
[45] G. Nyström, A. Marais, E. Karabulut, L. Wågberg, Y. Cui, M. M. Hamedi, *Nat. Commun.* **2015**, *6*, 7259.
[46] P. Yang, D. Chao, C. Zhu, X. Xia, Y. Zhang, X. Wang, P. Sun, B. K. Tay, Z. X. Shen, W. Mai, H. J. Fan, *Adv. Sci.* **2016**, *3*, 1500299.
[47] Q. Kong, L. Zhang, M. Wang, M. Li, H. Yao, J. Shi, *Sci. Bull.* **2016**, *61*, 1195.
[48] L. Dong, G. Liang, C. Xu, W. Liu, Z. Pan, E. Zhou, F. Kang, Q. Yang, *Nano Energy* **2017**, *34*, 242.
[49] H. Sun, S. Xie, Y. Li, Y. Jiang, X. Sun, B. Wang, H. Peng, *Adv. Mater.* **2016**, *28*, 8431.

